J Sol-Gel Sci Technol (2008) 45:261–267
DOI 10.1007/s10971-007-1674-z

ORIGINAL PAPER

Improvement of the bioactivity of organic–inorganic hybrid aerogels/wollastonite composites with TiO_2

J. A. Toledo Fernández · R. Mendoza-Serna · A. Santos · M. Piñero · N. de la Rosa-Fox · L. Esquivias

Received: 27 August 2007 / Accepted: 20 December 2007 / Published online: 23 January 2008

Abstract Organic–inorganic hybrid aerogels containing P and Ti have been synthesized by supercritical drying of alkogels prepared by hydrolysis and poly-condensation of metalo-organic precursors under high-power ultrasound. These materials become bioactive when doped with Ca. Wollastonite particles ($CaSiO_3$) were added as an active phase, instead of incorporating Ca into the aerogel atomic network. These particles had previously been precipitated and were then added to the sol. The aerogels were studied by Fourier transform infrared analysis, scanning electron microscopy coupled with energy dispersive spectroscopy and X-ray diffraction and N_2 adsorption. The stress–strain behaviours were evaluated under compression to obtain the Young's modulus. It was found that the incorporation of TiO_2 into wollastonite-P_2O_5 hybrid aerogels increased their capacity to form apatite and, consequently, improving their bioactive response.

J. A. Toledo Fernández · R. Mendoza-Serna · N. d. l. Rosa-Fox
Departamento de Física de la Materia Condensada, Facultad de Ciencias, Universidad de Cádiz, Cadiz, Spain

A. Santos
Departamento de Cristalografía y Mineralogía. CASEM, Universidad de Cádiz, Cadiz, Spain

M. Piñero
Departamento de Física Aplicada, CASEM, Universidad de Cádiz, Cadiz, Spain

L. Esquivias (✉)
Departamento de Física de la Materia Condensada, Facultad de Física, Instituto de Ciencia de Materiales de Sevilla (CSIC), Universidad de Sevilla, Avenida Reina Mercedes, s/n, 41012 Sevilla, Spain
e-mail: luisesquivias@us.es
URL: www.uca.es/grup-invest/geles

Keywords Organic–inorganic hybrid · Aerogel · Wollastonite · Composite · Bioactive materials · Mechanical properties

1 Introduction

Organic–inorganic hybrid materials (OIHM) are being used for implants since they are tolerated by the human organism; a fibrous tissue is created when they are embedded in the body. However, they do not become bonded to the bone unless they are bioactive. In such case, a layer of hydroxycarbonate apatite (HCA) grows and envelops the material when it is immersed in blood plasma or in solutions mimicking the properties of plasma [1]. One of the routes proposed for making OIHM incorporates the organic phase in the inorganic precursor sol under ultrasound assistance [2]. The two phases become chemically bonded after gelation and the resulting product is known as hard ormosil®, also called sono-ormosil. These gels are denser and less porous, and present better thermal stability, than those prepared by the classic procedure [3]. This approach to the biomineralization process combines the particular advantages of the organic polymers, such as flexibility, low density, toughness and formability, and other specific characteristics, such as their hydrophobic/hydrophilic features and porosity control, with the surface hardness and modulus strength contributed by the inorganic component. A low concentration of the organic phase is sufficient to improve the mechanical performance of the dry gel while only slightly diminishing the Si–OH surface coverage, which is necessary for the formation of the apatite layer [4].

Bioactivity is enhanced in ormosils containing calcium. When Ca is added to the initial sol from a salt, most of the Ca(II) is eliminated during drying because it is removed

together with the solvent [5]. With the purpose of avoiding the elimination of Ca(II) and subsequently modifying the mechanical behaviour of the gel, we have added Ca in the form of wollastonite ($CaSiO_3$) particles, since this mineral exhibits good bioactivity and biocompatibility [6, 7].

Aerogels can be used as the structural support for various different active phases [8]. In previous work, we have added wollastonite to the precursor sol, and bioactive silica-based aerogels are obtained after chemical drying. The presence of phosphorus induces the crystallization of a larger number of phases and stabilizes the wollastonite phase at high temperature [9].

The SiO_2–CaO–P_2O_5 system has been chosen as the inorganic phase because it promotes the bonding of bioactive glasses to both soft and hard tissue without forming an intermediate fibrous layer, and gives satisfactory results in in vivo implantation [10]. Hydroxyapatite/titania hybrid coating on Ti substrate has shown to combine the adhesion strength of TiO_2 [11]. The sol–gel method permits the synthesis of materials with higher purity and homogeneity at low processing temperature [12].

Titania gel was found to form a bone-like apatite on its surface in simulated body fluid (SBF), in a similar way to a silica gel [13]. Various kinds of bioactive materials with different mechanical properties have been developed based on titania. Titanates generally show a higher elastic modulus and better chemical durability than silicates and phosphates. Bioactive materials based on titania are, therefore, expected to exhibit properties that are different from those of bioactive materials based on silicates and phosphates [13].

The object of the present work is to investigate the role of TiO_2 in a P_2O_5–SiO_2/poly-dimethyl-siloxane (PDMS) aerogel matrix to improve the bioactivity of an aerogel/wollastonite composite OIHM, and to evaluate their mechanical properties.

2 Processing and experimental methods

2.1 Processing of wollastonite powders

Wollastonite powders were prepared by the precipitation method and subsequent heat treatment. Calcium nitrate ($Ca(NO_3)_2 \cdot 4H_2O$) (Aldrich Chemical Co., USA; purity 99%) and tetraethyl orthosilicate (TEOS: $Si(OC_2H_5)_4$) (Merck, Germany; purity ≥99%) were used as precursors. Both reagents were dissolved in 0.5 L of EtOH (Panreac, Spain; 99.5%) adjusting the concentration to 0.2 mol of $Ca(NO_3)_2 \cdot 4H_2O$ and 0.2 mol of TEOS. A precipitate was obtained by adding 0.33 mol/L of NaOH (Probus, Spain; 97%) solution. The powder was extracted by centrifugation, washed (several times) in distilled water and ethanol and finally dried at 100 °C for 24 h. Once dried, the powders were heat-treated in air at 1,000 °C for 2 h; the heating rate was 3 °C/min. Prior to their inclusion in the gel, the powder surface was chemically modified with 3-aminopropyltrimethoxysilane (Fluka, France; ≥97%) in order to facilitate and stabilize the dispersion of the colloid in the host matrix.

2.2 Processing of the composite SiO_2–CaO–P_2O_5 (W–P)

Tetraethyl orthosilicate and trimethyl-phosphate (PO$(CH_3O)_3$) (Aldrich Chemical Co., USA; >99%) were used as SiO_2 and P_2O_5 precursors, respectively, to prepare the hybrid gel matrix. TEOS was dissolved in 2 mL of EtOH in a molar ratio [TEOS]:[EtOH] = 0.66 (Solution A). A two-stage hydrolysis was performed as follows: TEOS was first partially hydrolysed (pH ~ 0) with HNO_3 catalyst in a molar ratio of [TEOS]:[H_2O] = 1:1.09. At this stage, 320 J/cm^3 of ultrasound was applied to the mix from a device delivering 0.6 W/cm^3 of ultrasound power energy to the system, resulting a transparent and homogeneous solution. In spite of the hydrolysis rate of the phosphorous alkoxide is lower than that of TEOS, then 0.0064 mol of trimethyl-phosphate was added to the sol because this was the sequence that gave the best results regarding apparent homogeneity. Silanol-terminated PDMS with quoted average molecular weight of 400–700 g/mol (ABCR, USA; 99.5%) was used as the polymer component. This organic polymer was added (drop by drop, under the action of 320 J/cm^3 of ultrasound) in a molar ratio [TEOS]:[DMS] = 1:0.027 (representing 19% by weight of PDMS with respect to the final amount of silica), where the organic fraction has been expressed as a function of the dimethyl-siloxane monomer, DMS. Then the sol was left in an oven for 24 h at 50 °C. The mix was hydrolysed (pH ~ 1) with HNO_3 catalyst (Panreac, Spain; 60%) in a molar ratio [TEOS]:[H_2O] = 1:4.08, applying again 320 J/cm^3 of ultrasound energy. Finally, 1.71 g of wollastonite powder was dispersed in 7 mL of EtOH and then added to the precursor sol under sonication (320 J/cm^3). The mixture was poured into a polyethylene container before gelation, which occurs in approximately 1 min, thus preventing the powder from settling. Then the container was left in an oven at 50 °C for 24 h. Next, the alkogels were soaked in ethanol at room temperature for 7 days. The [SiO_2]:[CaO]:[P_2O_5] molar ratios of this composite (designated W–P) are 9.43:2.22:1.

2.3 Processing of the composite SiO_2–CaO–P_2O_5–TiO_2 (W–P–Ti)

Titanium ethoxide ($Ti(OC_2H_5)_4$) (Aldrich Chemical Co., USA; 99.5%) was used as TiO_2 precursor. This reagent was chelated with acetylacetone (2,4-pentanedione, acacH) (Merck, Germany; >99%) to slow down its high hydrolysis

rate [14, 15]. Then 0.65 mL of titanium alkoxide was diluted in an ethanol and acacH mixture according to the molar ratio $[Ti(OEt)_4]$:[AcacH]:[EtOH] = 1:1.6:11 under 320 J/cm^3 of ultrasound energy (Solution B). Solutions A and B were mixed and hydrolysed (pH ~ 0) with HNO_3 catalyst in a molar ratio of [TEOS]:$[H_2O]$ = 1:1.09 with the application of 320 J/cm^3 of ultrasound energy. Immediately after, 0.0064 mol of trimethyl-phosphate was added to this sol. Then the organic polymer was added in the same way as described in the preceding paragraph. Then the resulting sol was left in an oven for 24 h at 50 °C before being hydrolysed (pH ~ 1) with HNO_3 catalyst with [TEOS]:$[H_2O]$ = 1:4.08, again under sonication (320 J/cm^3). Finally, the wollastonite powder was added to this sol and this mixture gelled in approximately 5 min. Then the gel was treated in the same way as before. The $[SiO_2]$:[CaO]:$[P_2O_5]$:$[TiO_2]$ molar ratios of this composite (designated W–P–Ti) are 9.43:2.22:1:0.81.

2.4 Drying and characterization

Both types of wet composite were dried by a supercritical drying process. They were placed in an autoclave (capacity 500 mL) and covered with an amount of ethanol sufficient for the critical pressure of ethanol to be exceeded at the critical temperature. Then the temperature was slowly raised at 1 °C/min until $T = 252$ °C, resulting in an increase in pressure to 78 atm. These conditions were maintained for half an hour. The experimental details have been reported elsewhere [3].

In order to evaluate the bioactivity, the aerogels were immersed in sterile polyethylene boxes containing SBF at 37 °C and soaked for 20 days, according to the procedure proposed by Kokubo et al. [16]. Then the aerogels were rinsed with distilled water and dried at 50 °C for 24 h. The Fourier transform infrared (FTIR) spectra of the aerogels were recorded after soaking in a Bruker Vertex70 spectrophotometer with a resolution of 4 cm^{-1} in the 2,000–400 cm^{-1} region. Pellets were prepared by grinding the samples in an agate mortar and then mixing the powder with anhydrous KBr in a weight ratio KBr:sample = 100:1. The formation of apatite-like layers on the surfaces of the disks was monitored by scanning electron microscopy (SEM) in a FEI Sirion electron microscope coupled to an EDAX Genesis system. The thermogravimetric (TG) study was carried out in a Setaram Setsys 1750 by heating the samples in air from 25 to 1,000 °C at 10 °C/min. The average pore diameter and surface area of the aerogels were determined by N_2 adsorption/desorption isotherms at 77 K carried out in a Sorptomatic 1990 (CE Instruments) equipment. The X-ray diffraction (XRD) measurements were performed in a Bruker AXS D8 Advance diffractometer by the step-scanning method with Cu K_α radiation, a scan range between 20 and 50° 2θ, with a step of 0.2°, and a counting time of 1 s per step; the instrument was operated at 40 kV and 40 mA. The strains at failure of the aerogels were evaluated at room conditions under compression with an AG-I machine (Shimadzu); the Young's moduli were calculated from the slope of the initial linear elastic portion of the stress-strain curve.

In vitro assays were carried out soaking the aerogels in 40 mL of SBF at 37 °C for 20 days. SBF is an aqueous acellular solution with ionic composition almost equal to human plasma [17]: Na^+, 142; K^+, 5.0; Mg^{2+}, 1.5; Ca^{2+}, 2.5; Cl^-, 147.8; HCO_3^-, 4.2; HPO_4^{2-}, 1.0 and SO_4^{2-}, 0.5 mM, buffered at pH 7.4 with tris-hydroxymethyl aminomethane/HCl 1 M [18].

3 Results and discussion

Figure 1 is an SEM image of wollastonite powder particles, in which their acicular texture can be observed. The approximate width of the aciculae that form the synthesized wollastonite particles is a few tenths of nm. This aspect of the particles has been carefully examined and reported previously [19].

The FTIR spectra of the aerogels are shown in Fig. 2. The corresponding assignments are given in Table 1. The bands relating to the CO_3^{2-} group for FTIR show that the PO_4^{3-} ions are substituted in the HA by the carbonate ions according to the HCA structure. The HCO_3^- band at ~1,635 cm^{-1} overlaps with that of the molecular H_2O absorbed during immersion in the SBF. This may not be attributable solely to water (although it may well be, since the PDMS content is only 19% by weight) because of the hydrophobicity of OIHM. The 1,065 and 1,074 cm^{-1}

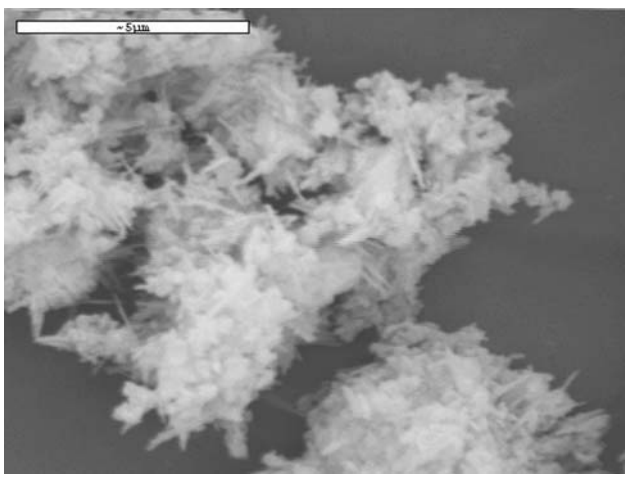

Fig. 1 SEM image of the wollastonite powders

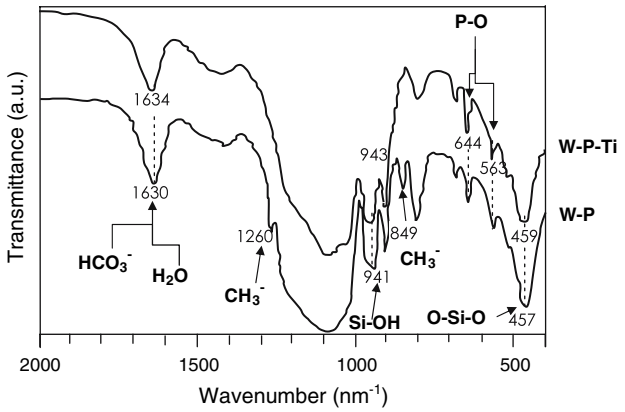

Fig. 2 FTIR spectra of W–P and W–P–Ti aerogels after soaking in SBF

Table 1 FTIR bands assignments of W–P and W–P–Ti aerogels

Assignment	Wavenumber (cm^{-1})	
	W–P	W–P–Ti
HCO_3^- [20] and H_2O [21]	1,630	1,634
v_3 CO_3^{2-} [21–23]	1,396	1,410
P=O [24]	1,250	
Si–O and P–O stretching [20, 21]	1,065	1,074
Si–OH [25, 26]	957–941	943
PDMS [27]	903	905
P–O(H) stretching [28, 29]	849	
v_4 CO_3^{2-} [18]	679	681
P–O bending of HA [21, 22, 30]	644	644
	563	563
O–Si–O bending [25]	457	459

bands should be the result of the superposition of Si–O and P–O stretching [20, 21] for W–P and W–P–Ti, respectively. The presence of Si–OH bands in W–P and W–P–Ti aerogels in the 960–940 cm^{-1} region is reported to be essential for the formation of HCA [31]. Téllez et al. [32] have reported that in hybrid materials prepared through the reactions of Si and Ti alkoxides and polydimethil siloxane (PDMS), the polycondensation reaction between Si–OH groups and PDMS molecules can be monitored by the 850 cm^{-1} band. They have shown that the formation of 3-D structures bonds Si–O–Si by the titanium alkoxide but, on the contrary, this hinders the TEOS-PDMS co-polymerization reaction. This band is absent in the W–P–Ti samples; at the same time, there can be observed in the W–P sample spectrum an absorption peak at 1,260 cm^{-1} that is attributed to methyl groups, seemingly belonging to the phosphorous alkoxide precursor. The absorption peak at around 800 cm^{-1} was assigned to CH_3 groups derived from PDMS [33], and to the presence of phosphorous in the hybrid network [34].

The fact that the IR bands at ~940 and 560 cm^{-1} (relative to Si–OH and Si–O groups) are systematically weaker for the W–P–Ti sample shows that the Ti induces a more reticulated structure. This conclusion is reinforced by the fact that the W–P sample retains amounts of unreacted organic groups. These structural conditions before soaking in SBF favour the formation of tiny HCA particles on the surface of the W–P–Ti sample once it is immersed in the fluid.

Figures 3 and 4 show SEM micrographs of the surfaces of W–P and W–P–Ti aerogels, respectively, after soaking in SBF for 20 days. Their respective XRD patterns are represented in Fig. 5. The W–P sample features the reflections of the wollastonite [35] as well as weak reflections at $2\theta = 31.7$, 32.2, 34.1 and 39.2 corresponding to *syn* hydroxyapatite (Pattern: 01-086-1203) [36, 37] that cannot be in seen in its W–P–Ti counterpart. The diffraction profiles show that the crystallinity of the hydroxyapatite is less

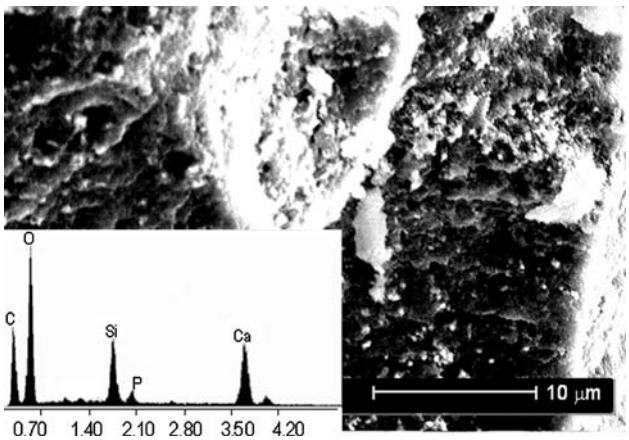

Fig. 3 SEM micrograph and EDS pattern of the W–P composite after soaking in SBF

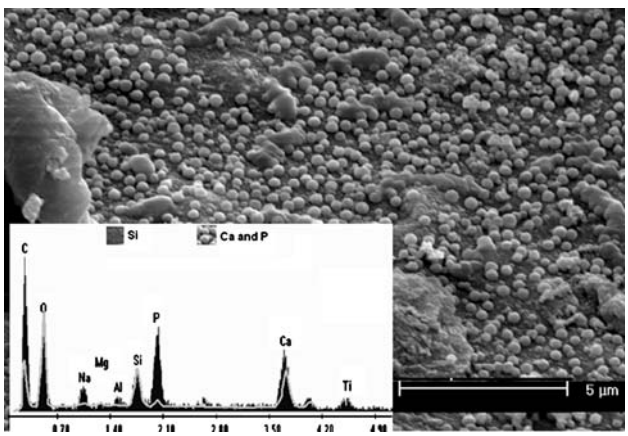

Fig. 4 SEM micrograph and EDS pattern of the W–P–Ti composite after soaking in SBF. The grey line is the normalized pattern of the W–P sample

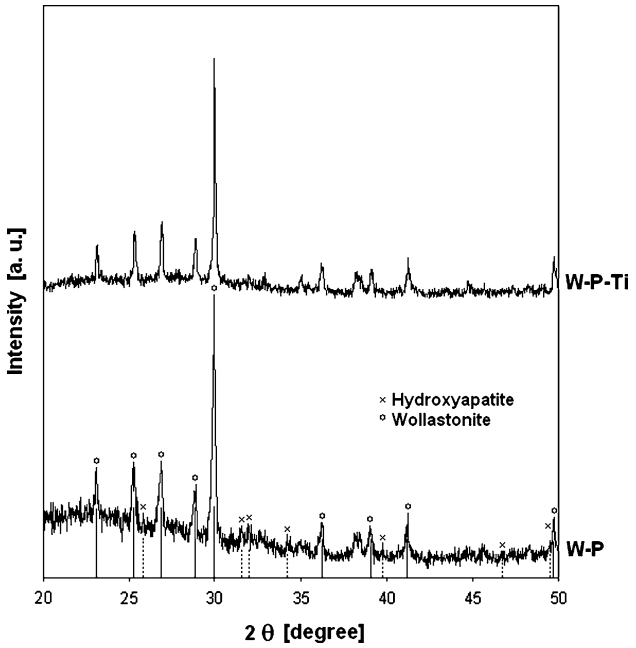

Fig. 5 X-ray powder diffraction patterns for W–P and W–P–Ti aerogels

when Ti is present. From this diffractogram it is not possible to confirm the presence of hydroxyapatite in the W–P–Ti sample. However the FTIR 653 cm^{-1} band, which is usually attributed to the P=O of the hydroxyapatite, is well resolved. On the other hand, the hydroxyapatite morphology is similar to that of the particles shown in Fig. 4.

However, no particles can be identified on the rough surface of the W–P aerogel (Fig. 3). In contrast, spherical-shaped apatite particles of 0.3–0.4 μm diameter are observed on the surface of W–P–Ti aerogel (Fig. 4). In the W–P sample, fewer hydroxyapatite nuclei are formed than in the W–P–Ti sample, as can be inferred from the energy dispersive spectroscopy (EDS) analysis. The crystal size in this sample, calculated from Scherrer's equation, is estimated to be ~20–30 nm. In the W–P–Ti sample, the Ti induces the nucleation of the hydroxyapatite, reducing the time before nucleation occurs and increasing the flow for nucleation. The hydroxyapatite particles in the W–P–Ti sample measured in the SEM micrograph are larger than 300 nm. This crystal size would be large enough to give rise to well-resolved peaks in the XRD pattern. Consequently, those particles have to be amorphous.

For the sake of clarity, we have normalized the EDS patterns with reference to the Si peak (Fig. 3). It can be seen that Si and O present the same relative intensities. The most relevant feature is the high P peak that appears in the W–P–Ti sample in comparison with its W–P counterpart. However, the amount of Ca in the W–P sample is only slightly less than that in the W–P–Ti. The [Ca]:[P] ratio calculated in the W–P sample is much higher than the nominal contents of both the hydroxyapatite and the composite. Curiously, however, in the W–P–Ti sample the [Ca]:[P] ratio = 1.65, nearly matching the value in the stoicheiometric hydroxyapatite $Ca_{10}(PO_4)_6(OH)_2$ [6, 38], which grows by consuming the calcium and phosphate ions of the SBF. We consider that these very different [P] values are due only to the inhomogeneous distribution of this element in the aerogel matrix when trimethyl-phosphate is used as precursor [39]. For this reason we take the [Ca]:[Si] ratio as a more plausible reference of the presence of hydroxyapatite on the surface. This ratio is 51% higher in the sample containing Ti than in the W–P sample. Consequently, this fact, together with the evidence of the hydroxyapatite particles on the surface of the W–P–Ti, indicates that the incorporation of TiO_2 into the atomic network increases the apatite nucleation on the surface.

These materials exhibited characteristics of types IV and V isotherms (Fig. 6) that correspond to mesoporous materials, in which the N_2 adsorption at low pressure is produced by the formation of multiple layers. At high pressure, the adsorption is caused by capillary condensation, which is characterized by a clear hysteresis loop occurring in the mesoporous range. A transition is observed in the hysteresis loops from H4 to H3 type, which indicates the presence of pores formed by flattened particles and slit-shaped pores, respectively, as Ti is incorporated into the matrix atomic network. This reveals that Ti addition significantly modifies the pore structure of the gel network. Specifically, the Ti-free aerogel showed an H4 hysteresis loop. This loop seems to be due merely to the existence of mesopores formed by the organic phase embedded within the inorganic phase containing relatively few micropores. Microporosity is a characteristic of silica aerogels, which is modified by the presence of the organic phase [40]. In fact,

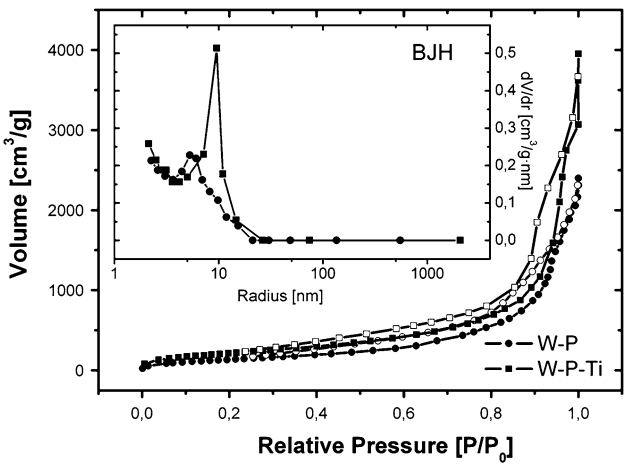

Fig. 6 Nitrogen adsorption/desorption isotherms for W–P and W–P–Ti aerogels. In the inset is represented their respective pore size distribution according to the BJH method

the isotherms do not show a completely linear behaviour at low pressure: there is a slight increase of adsorbed volume at $P/P_o < 0.04$, typical of microporous solids. Also, the extent of the hysteresis loop indicates a very slow desorption of N_2 in the low P/P_o region. This corroborates the conclusion that a few micropores remain in the matrix of the inorganic phase. The W–P–Ti sample presents the H3 type but with some features of the H4 loop, which is characterized by saturation not being reached. It reveals a loose assemblage between particles and the matrix, promoting the appearance of slit-like pores. Isotherms corresponding to the W–P sample show instead an H3 hysteresis loop, which indicates a tendency towards a reduced aggregation between phases and, subsequently, towards an increased pore size.

The pore size distribution in the mesoporous zone was evaluated using the method proposed by Barret, Joyner and Halenda (BJH) [41] (inset in Fig. 6). Table 2 summarizes the results extracted from these analyses. The BET surface area of the W–P and W–P–Ti aerogels was 539 and 812 m^2/g, respectively.

The derivative of the weight loss thermograms (DTG) curves for the W–P and W–P–Ti aerogels are shown in Fig. 7. The thermograms present differences in their respective contents of water after soaking in SBF. The DTG curve of aerogels after 20 days in SBF display this feature at ≈ 100 °C, which corresponds to the elimination

Table 2 Textural data for the W–P and W–P–Ti aerogels

Aerogel	BET surface area (m^2/g)	Average pore diameter (nm) (BJH)
W–P	539.3	3.3
W–P–Ti	812.4	20.6

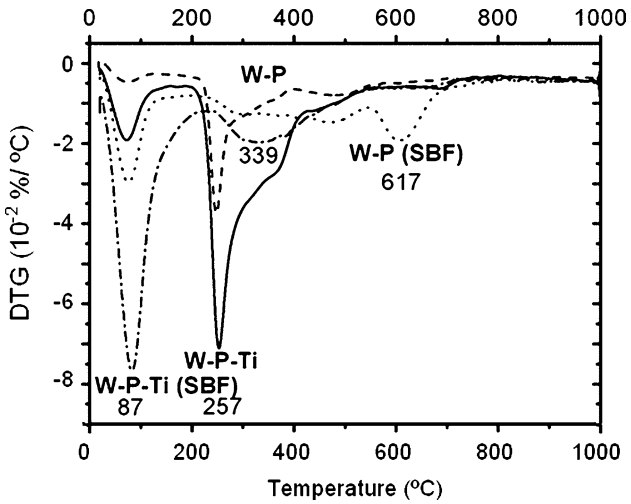

Fig. 7 DTG curves for aerogels after soaking in SBF

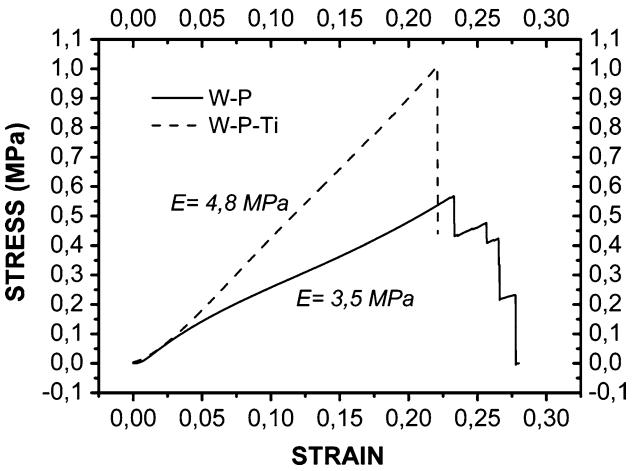

Fig. 8 Stress–strain curves for W–P and W–P–Ti aerogels

of its high water content [42]. The second weight loss (250–350 °C) corresponds basically to the removal of organic residuals, which is more important in the aerogels after soaking in SBF. The W–P–Ti aerogel presents a greater weight loss in this temperature interval than the W–P aerogel, both after and without soaking in SBF.

Figure 8 shows the stress–strain curves of the aerogels. The Young's modulus increases from 3.5 to 4.8 MPa when Ti is incorporated into the inorganic network. This value remains constant independently of the strain, whereas in the W–P sample the Young's modulus decreases with increasing strain. The strain at failure also increases, from 0.56 (W–P) to 1.0 MPa (W–P–Ti).

Consequently, the incorporation of TiO_2 into the matrix network favours the crystallization of the hydroxyapatite, thus increasing both the resistance to fracture and the Young's modulus [43, 44].

4 Conclusion

1. The incorporation of TiO_2 into the SiO_2–CaO–P_2O_5/PDMS atomic network increases the specific surface area and average pore diameter of the aerogels and, after the sample has been immersed in SBF, gives rise to spherical shaped apatite particles of 0.3–0.5 μm diameter.
2. After soaking in SBF, the aerogels lose less organic polymer than the same aerogels before soaking.
3. The incorporation of TiO_2 into the atomic network increases its bioactivity; the resistance to fracture remains constant and the Young's modulus against strain increases and stabilizes.

Acknowledgements The authors are grateful to the Spanish Ministerio de Educación y Ciencia and the Consejería de Innovación

Ciencia y Empresa of the Junta de Andalucía (Spain) (Projects MAT2005-01583 and TEP 790, respectively), for the financial support provided. R. Mendoza-Serna thanks the U.N.A.M., DGAPA, México, for the scholarship supporting his sabbatical stay at the Departamento de Física de la Materia Condensada, Facultad de Ciencias, Universidad de Cádiz.

References

1. Krupa D, Baszkiewicz J, Kozubowski JA, Barcz A, Sobczak JW, Bilinski A, Lewandowska-Szumiel M, Rajchel B (2005) Biomaterials 26:2847
2. Mackenzie JD (1994) J Sol–Gel Sci Tech 2:81
3. de la Rosa-Fox N, Esquivias L, Piñero M (2003) In: Nalwa SH (ed) Handbook of organic–inorganic hybrid materials and nanocomposites, vol. 1. American Scientific Publishers, CA, pp 241
4. Chen Q, Miyata N, Kokubo T, Nakamura T (2000) J Biomed Mater Res 51(4):605
5. Esquivias L, Morales-Flórez V, Piñero M, de la Rosa-Fox N, Ramírez J, González-Calbet J, Salinas A, Vallet-Regí M (2005) Mater Res Soc Symp Proc 847:EE12.1
6. Liu X, Ding Ch, Chu PK (2004) Biomaterials 25:1755
7. de Aza PN, Aza AH, de Aza S (2005) Bol Soc Esp Ceram V 44(3):89
8. Suslick KS (1997) In: Ertl G, Knözinger H, Weitkamp J (eds) Handbook of heterogeneous catalysis. VCH, p 1350
9. Padilla S, Román J, Carenas A, Vallet-Regí M (2005) Biomaterials 26:475
10. Balamurugan A, Sockalingum G, Fauré J, Banchet V, Wortham L, Bouthors S, Laurent-Maquin D, Balossier G (2006) Mater Lett 60:3752
11. Im JK-H, Lee S-B, Kim K-M, Lee Y-K (2007) Surf Coat Technol. Available on line doi:10.1016/j.surfcoat.2007.07.081
12. Lao J, Nedelec JM, Moretto Ph, Jallot E (2007) Nucl Instrum Methods Phys Res B 261:488
13. Kokubo T, Matsushita T, Takadama H (2007) J Eur Ceram Soc 27:1553
14. Léaustic A, Babonneau F, Livage J (1989) Chem Mater 1(2):240
15. Léaustic A, Babonneau F, Livage J (1989) Chem Mater 1(2):248
16. Kokubo T, Kushitani H, Sakka S, Kitsugi T, Yamamuro T (1990) J Biomed Mater Res 24(6):721
17. Martin AI, Salinas AJ, Vallet-Regí M (2005) J Eur Ceram Soc 25:3533
18. Kokubo T, Takadama H (2006) Biomaterials 27:2907
19. Santos A, Toledo-Fernández JA, Mendoza R, Gago-Duport L, de la Rosa-Fox N, Piñero M, Esquivias L (2007) Ind Eng Chem Res 46:103
20. Branda F, Fresa R, Costantini A, Buri A (1996) Biomaterials 17:2247
21. Ricardo Costa OR, Marivalda Pereira M, Fernando Lameiras S, Wander Vasconcelos L (2005) J Mater Sci-Mater M 16:927
22. Rámila A, Vallet-Regi M (2001) Biomaterials 22:2301
23. Nakamoto K (1997) Infrared and Raman spectra of inorganic and coordination compounds, Part A: theory and applications in inorganic chemistry, 5th edn. Wiley, p 359
24. Liu D-M, Yang Q, Troczynski T, Tseng WJ (2002) Biomaterials 23:1679
25. Jung HY, Gupta RK, Oh EO, Kim YH, Whang CM (2005) J Non-Cryst Solids 351:372
26. Lee K-Y, Lee Y-H, Kim H-M, Koh M-Y, Ahn S-H, Lee H-K (2005) Curr Appl Phys 5:453
27. Téllez L, Rubio J, Rubio F, Morales E, Oteo JL (2004) Spectrosc Lett 37:11
28. Ning CQ, Greish Y, El-Ghannam A (2004) J Mater Sci-Mater M 15:1227
29. Pleshko N, Boskey A, Mendelsohn R (1991) Biophys J 60:786
30. Xianghui W, Chengkang C, Dali M, Ling J, Ming L (2005) Mater Sci Eng C 25:455
31. Alemany MI, Velasquez P, de la Casa-Lillo MA, De Aza PN (2005) J Non-Cryst Solids 351:1716
32. Téllez L, Rubio F, Peña-Alonso R, Rubio J (2004) Bol So Esp Ceram 43(5):883
33. Yabuta T, Tsuru K, Hayakawa S, Osaka A (2004) J Sol–Gel Sci Tech 31:273
34. Manzano M, Salinas AJ, Vallet-Regí M (2006) Prog Solid State Chem 34:267
35. Sreekanth Chakradhar RP, Nagabhushana BM, Chandrappa GT, Ramesh KP, Rao JL (2006) Mater Chem Phys 95:169
36. Aburatani Y, Tsuru K, Hayakawa S, Osaka A (2002) Mater Sci Eng C 20:195
37. Kamitakahara M, Kawashita M, Miyata N, Kokubo T, Nakamura T (2002) J Mater Sci-Mater M 13:1015
38. Liu X, Ding Ch, Wang Z (2001) Biomaterials 22:2007
39. Fernández-Lorenzo C, Esquivias L, Barboux P, Maquet J, Taulelle F (1994) J Non-Cryst Solids 176:189
40. Morales-Flórez V (2007) Modelos Estructurales y Propiedades Mecánicas de Aerogeles Híbridos. Ph D Thesis, University of Seville, Spain
41. Barrett EP, Joyner LG, Halenda PP (1951) J Am Chem Soc 73:373
42. Wan X, Chang Ch, Mao D, Jiang L, Li M (2005) Mater Sci Eng C 25:455
43. Chen Q, Miyata N, Kokubo T, Nakamura T (2001) J Mater Sci-Mater M 12:515
44. Miyata N, Fuke K-I, Chen Q, Kawashita M, Kokubo T, Nakamura T (2004) Biomaterials 25:1